D. Corinti, A. De Petris, C. Coletti, N. Re, B. Chiavarino, M. E. Crestoni, S. Fornarini, *ChemPhysChem* **2017**, *18*, 318.

Cisplatin Primary Complex with L-Histidine Target Revealed by IRMPD Spectroscopy

Davide Corinti,[a] Alberto De Petris,[a] Cecilia Coletti,[b] Nazzareno Re,[b] Barbara Chiavarino,[a] Maria Elisa Crestoni,[a] and Simonetta Fornarini*[a]

Abstract: The primary complex obtained from cisplatin and L-histidine in water has been detected and isolated by electrospray ionization. The so-obtained cis-[PtCl$(NH_3)_2$(histidine)]$^+$ complex has been thoroughly characterized by high resolution mass spectrometry (MS), tandem MS, IR multiple photon dissociation (IRMPD) spectroscopy and quantum chemical calculations. The structural features revealed by IRMPD spectroscopy indicate that platinum binds to the imidazole group, which presents tautomeric forms. Thus, depending on the position of the amino acid pendant on the imidazole ring, isomeric complexes are formed that are remarkably different in their ease to undergo fragmentation, when activated either by energetic collisions or by multiple IR photon absorption. It is shown here how IRMPD kinetics can allow an estimate of their relative proportions.

Introduction

Cisplatin (*cis*-diaminedichloroplatinum(II)) is the premier compound of a family of Pt complexes successfully used as antitumor drugs and is nowadays still largely present in chemotherapeutics.[1-3] While the mechanism of action, involving entry into the cell and aquation steps ultimately leading to nucleobase binding and DNA distortion, is known well enough,[4,5] fewer details are available on the interaction of cisplatin with other molecules in the biological medium. Indeed, cisplatin has been found to bind to a variety of biological targets,[6] notably amino acid residues in peptides and proteins.[7,8] Some data indicate that cisplatin interaction with proteins, held responsible for toxic side effects, may also account for antitumor activity.[7] The reaction of cisplatin with L-histidine (His), a prime target together with S-containing amino acids, has been found to yield a variety of compounds in which His is coordinated to the metal via an imino N or amino N atom.[9] The His donor atom for diammine Pt^{II} complexes may also include a carboxylate oxygen and the coordination pattern tends to evolve forming stable chelate complexes.[10] However, the early complex *cis*-[PtCl$(NH_3)_2$(His)]$^+$ from the first substitution event, either directly on cisplatin or on the intermediate aqua complex *cis*-[PtCl$(NH_3)_2(H_2O)]^+$, has never been observed. Electrospray ionization mass spectrometry (ESI-MS) affords the means to extract ionic species from solution to the gas-phase where they can be selectively isolated and characterized. Herein, a thorough characterization of the *cis*-[PtCl$(NH_3)_2$(His)]$^+$ complex is presented, based on IR multiple photon dissociation (IRMPD) spectroscopy combined with quantum chemical calculations.[11-13] This integrated approach has enabled us to unveil chemical properties of cisplatin derived complexes relevant for the drug biological activity, namely vibrational features of the naked early aqua complex, nucleobase and nucleotide interaction, ligand substitution within the Eigen-Wilkins encounter complex isolated from the aqueous medium.[14-17] A glycine-linked cisplatin complex, $[(Gly\text{-}H)PtCl_2]^-$, has also provided a case study for IRMPD experiments interpreted by a survey of hybrid theoretical approaches.[18] Metal ion (alkali metals, Cu^{II}, Zn^{II}, Cd^{II}) complexes with His ligand(s) have also been successfully assayed.[19-22]

Results and Discussion

cis-[PtCl$(NH_3)_2$(His)]$^+$ complexes are directly revealed by ESI-MS as distinct ionic products from the reaction of cisplatin and His (mass spectrum shown in Figure S1 in the Supporting Information, SI). The isotopic cluster at *m/z* 418 conforms to the calculated distribution as shown by the inset in Figure S1. The assignment is further verified by high resolution mass analysis confirming the elemental composition of the sampled ion as illustrated in Figure S2. In order to further ascertain the ion composition, collision induced dissociation experiments have been performed delivering variable energy to activate fragmentation in the intermediate collision sector of a triple quadrupole instrument. The prevailing dissociation channel

[a] Dr. D. Corinti, Prof. B. Chiavarino, Prof. M. E. Crestoni, Prof. S. Fornarini
Dipartimento di Chimica e Tecnologie del Farmaco
Università degli Studi di Roma La Sapienza
P.le A. Moro 5, I-00185 Roma, Italy
E-mail: simonetta.fornarini@uniroma1.it
[b] Prof. C. Coletti, Prof. N. Re
Dipartimento di Farmacia
Università G. D'Annunzio
Via dei Vestini 31, I-66100 Chieti, Italy

Supporting information for this article is given via a link at the end of the document.

involves loss of NH_3. Interestingly, however, the sampled *cis*-$[PtCl(NH_3)_2(His)]^+$ ions display a dual behavior (Figure S3). A fraction shows prompt fragmentation with NH_3 loss occurring already in the region preceding the collision quadrupole while a second component in the ion population is fairly resistant to dissociation. Structural characterization of what appears to be a mixture of isomers has been sought relying on the diagnostic power of IR spectroscopy of sampled gaseous ions as obtained by IRMPD spectroscopy supported by quantum chemical calculations.[11-13] Therefore, *cis*-$[PtCl(NH_3)_2(His)]^+$ ions are examined by IRMPD spectroscopy in two spectral ranges, namely 900-1900 cm^{-1} and 3000-3700 cm^{-1}, using the CLIO FEL and a tabletop OPO/OPA laser system as IR light sources, respectively.[23,24] The analysis of IRMPD spectra is aided by a comprehensive computational survey of the potential structures accounting for the sampled species and their respective calculated IR spectra. The results are illustrated in Figure 1 where panel A shows the experimental IRMPD spectrum in the two spectral regions. It is worth mentioning that IRMPD recorded in correspondence with active bands in the 900-1900 cm^{-1} 'fingerprint' range grows with irradiation time till almost complete (>95%) depletion of the parent ion abundance, implying good overlap of the laser beam with the ion cloud and efficient IRMPD activity as ensured by the high fluence of the FEL. The situation is different in the OPO/OPA range as illustrated in following paragraphs. Sampling in the 'fingerprint' range then accounts for the overall ion population. The experimental spectrum presents vibrational signatures which find a counterpart in the anharmonic IR spectra calculated for *cis*-$[PtCl(NH_3)_2(His)]^+$ structures where the metal is coordinated to an imino imidazole nitrogen (Figure 1 (B-E)). Figure 2 shows the optimized geometry of low energy conformers of two possible isomers arising from Pt binding to either one of the two N-atoms of the imidazole group. According to IUPAC recommendations,[25] they are named N_π (pros, near) and N_τ (tele, far), referring to their position relative to the side chain.

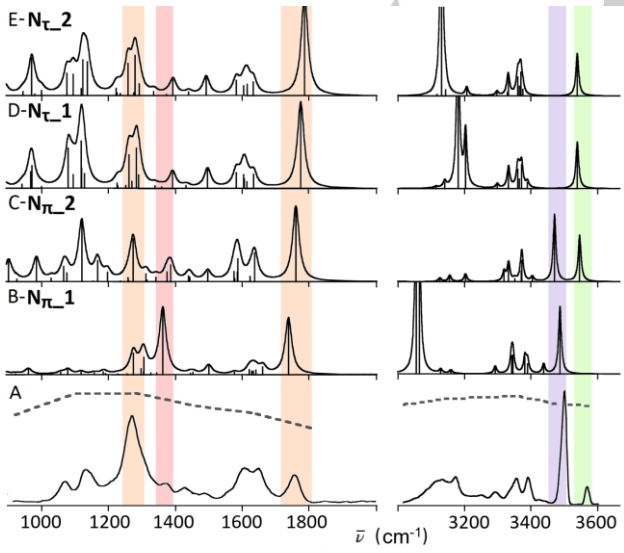

Figure 1. IRMPD spectrum of *cis*-$[PtCl(NH_3)_2His]^+$ (A) compared to the linear anharmonic IR spectra calculated at B3LYP/6-311+G** level of theory for the most stable conformers of N_π and N_τ families of isomers (B-E). The laser power along the recorded IRMPD spectrum is reported as dashed line.

Quantum chemical calculations have been performed at B3LYP/6-311+G** and also at ωB97X-D/6-311+G** level in order to account for dispersion contributions[26] and results are presented in Table 1 and in Table S1 in the SI.

While the ωB97X-D functional has proven good performances in the interpretation of the thermodynamic and geometrical features of Pt complexes[27], calculations of vibrational modes employing this functional should be viewed with caution. The harmonic IR spectra calculated at B3LYP/6-311+G** level have been compared with the corresponding ones obtained using the ωB97X-D hybrid functional. While no significant differences are observed (Figure S4), the frequency scaling factors (0.940 in the fingerprint range and 0.943 in the X-H stretching range) needed to provide adequate comparison of ωB97X-D calculated modes with the experimental absorptions suggest a poorer performance of the method in matching harmonic with experimental frequencies.

As shown by the data also reported in Figure 2, the inclusion of dispersion effects tends to widen the relative energy of **N_π** and **N_τ** isomers, favoring the more folded structures of **N_π_1** and **N_π_2**.

Table 1. Thermodynamic parameters for the most stable structures of N_π and N_τ conformers of *cis*-$[PtCl(NH_3)_2(His)]^+$ calculated at various levels of theory. Relative energies accounting for solvation effects are reported in brackets.

Species	Relative Energy (0K)[a]	Relative Enthalpy[a] (298K)	Relative Free Energy[a] (298K)
	B3LYP/6-311+G**		
Nπ_1	0.0	0.0 (0.0)	0.0 (0.0)
Nπ_2	3.4	4.4 (11.6)	4.7 (11.9)
Nτ_1	11.7	11.7 (8.0)	1.1 (-2.5)
Nτ_2	7.9	7.8 (3.7)	-1.5 (-5.6)
	ωB97XD/6-311+G**		
Nπ_1	0.0	0.0 (0.0)	0.0 (0.0)
Nπ_2	5.7	6.5 (14.0)	5.3 (12.7)
Nτ_1	33.1	32.1 (24.1)	18.8 (13.9)
Nτ_2	29.8	29.1 (27.6)	18.9 (14.3)
	B3LYP-D3/6-311+G**		
Nπ_1	0.0	0.0	0.0
Nπ_2	7.5	8.4	6.5
Nτ_1	34.3	33.9	20.8
Nτ_2	30.6	30.3	18.3
	MP2/cc-pVTZ(-PP)//B3LYP/6-311+G[b]**		
Nπ_1	0.0	0.0	0.0
Nπ_2	8.2	9.2	9.5
Nτ_1	29.6	29.5	20.2
Nτ_2	34.3	34.3	23.7

[a] In kJ mol^{-1}. [b] Zero-point energies and thermal corrections from B3LYP/6-311+G** calculations.

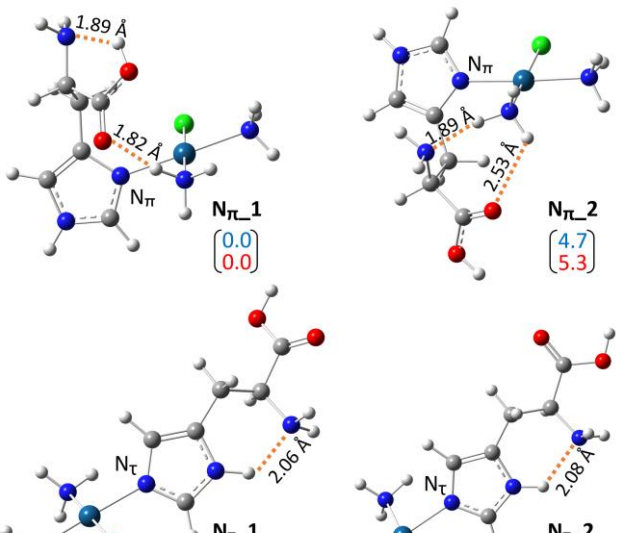

Figure 2. Calculated geometries of the most stable conformers of N_π and N_τ isomers of *cis*-$[PtCl(NH_3)_2His]^+$. Relative free energies (kJ mol^{-1}) calculated at B3LYP/6-311+G** (blue) and ωB97X-D/6-311+G** (red) level are reported in parentheses.

The significant effect on relative stability was confirmed employing the B3LYP-D3 functional and also performing single point energy calculations at the MP2/cc-pVTZ(-PP) level of theory on the geometries optimized with B3LYP/6-311+G**. The effect of solvation has also been considered and data accounting for it are given in parenthesis in Table 1. The inclusion of solvation consistently favors the less folded $\mathbf{N_\tau}$ isomers with respect to folded $\mathbf{N_\pi}$ species. This finding may be explained by the fact that $\mathbf{N_\pi}$ isomers are clearly less accessible to interactions with the solvent thus gaining less stabilization. Thermodynamic data for the lowest energy conformers are reported in Table 1 while a complete summary for all optimized geometries illustrated in Figure S5 can be found in Table S1.

It is to be noted, though, that once delivered to the gas-phase by the ESI process, $\mathbf{N_\pi}$ and $\mathbf{N_\tau}$ isomers are not expected to interconvert due to large isomerization barriers. In fact, an interconversion requires tautomerization of the imidazole unit, involving migration of a hydrogen atom from one nitrogen to the other. The search for a transition state for a synchronous process has, not unexpectedly, failed. Alternative stepwise isomerization paths require the cleavage of the Pt-bond to the imidazole imino nitrogen atom. The breaking of this bond may be assisted by the amino group attacking the metal in a five-coordinate transition state. The ensuing intermediate then resembles an amino-ligated isomer $\mathbf{N_aH_a}$ (Figure S6) which is calculated to lie at ca. 68 kJ mol^{-1} relative to $\mathbf{N_\pi\_1}$ (see Table S1). At this stage, the now freed imidazole group may undergo tautomerization in a process that, due to the absence of any solvent molecules, will require an intramolecular assistance. Thus, the N_π/N_τ isomerization is clearly a high energy process in the sampled isolated complexes. The underlying notion then is that the isomeric population characterized by IRMPD spectroscopy reflects the isomeric composition in solution. Inspection of the IRMPD spectrum in Figure 1A indicates that multiple species need to be involved to account for the observed features. Table S2 in the SI lists the observed IRMPD bands together with both the harmonic and the anharmonic vibrational modes calculated for the low energy conformers $\mathbf{N_\pi\_1}$, $\mathbf{N_\pi\_2}$, $\mathbf{N_\tau\_1}$, and $\mathbf{N_\tau\_2}$, representative of the two families of $\mathbf{N_\pi}$ and $\mathbf{N_\tau}$ isomers. While computationally demanding anharmonic calculations have been performed in the quest for an appropriate matching between the computed and experimental bands, one typically finds minor effects of the anharmonic treatment in the fingerprint region (900-1900 cm^{-1}). As expected, a significantly better agreement with the experiment is instead observed in the NH/OH stretches involved in hydrogen bonding interactions. In the IRMPD spectrum recorded in the fingerprint range, the C=O stretching band at 1755 cm^{-1} is better interpreted by the 1742-1763 cm^{-1} frequencies characteristic for species where the carbonyl group is involved in $NH^+ \cdots O{=}C$ hydrogen bonding, such as $\mathbf{N_\pi\_1}$ and $\mathbf{N_\pi\_2}$, rather than by the 1778-1789 cm^{-1} values for the nearly unperturbed carboxylic group in $\mathbf{N_\tau\_1}$, and $\mathbf{N_\tau\_2}$. A contribution of the latter species in the tail of the observed band cannot be discarded though. On the basis of the calculated IR spectra one may assign the unresolved bands at 1645 and 1607 cm^{-1} to asymm NH_3 bendings, the tiny band at 1492 cm^{-1} to in plane CH bending, the band at 1433 cm^{-1} to imidazole NH in-plane bending, the bands at 1375 cm^{-1} mainly to OH bending of $\mathbf{N_\pi\_1}$, the band at 1270 cm^{-1} to NH_3 umbrella modes, the band at 1133 cm^{-1} to a convolution of various modes including CH_2 twist and OH bend, and finally the band at 1075 cm^{-1} combines CN stretch with imidazole ring deformation modes. It has to be noted that the pronounced band at 1367 cm^{-1} in the calculated spectrum of $\mathbf{N_\pi\_1}$, corresponding to the OH bending mode, hardly appears to contribute, at least in terms of intensity, to the band observed at 1375 cm^{-1} in the IRMPD spectrum. However, failure of computed spectra to properly describe an OH bending mode involved in hydrogen bonding has already been noticed in previous works involving deprotonated and modified aminoacids.[28,29] Possibly, the non-linear character of the IRMPD process is responsible for this behavior which may arise from disruption of the H bond, intervening early along the multiple photon absorption sequence and hampering further resonant excitation. Incidentally, the presence of both $\mathbf{N_\pi}$ and $\mathbf{N_\tau}$ isomers is consistent with the fragmentation behavior upon CID if one recognizes that the N_π geometry may allow NH_3 loss leading to a chelate complex where the amino N atom (N_a) is the additional ligand ($[PtCl(NH_3)His(N_\pi,N_a)]^+$) while the N_τ geometry yields a three coordinate Pt complex in a considerably more energy demanding process (ca. 102 and 204 kJ mol^{-1}, respectively, see Table S1 for complete thermodynamic data and Figure S5 for geometries of species partaking in Scheme 1).

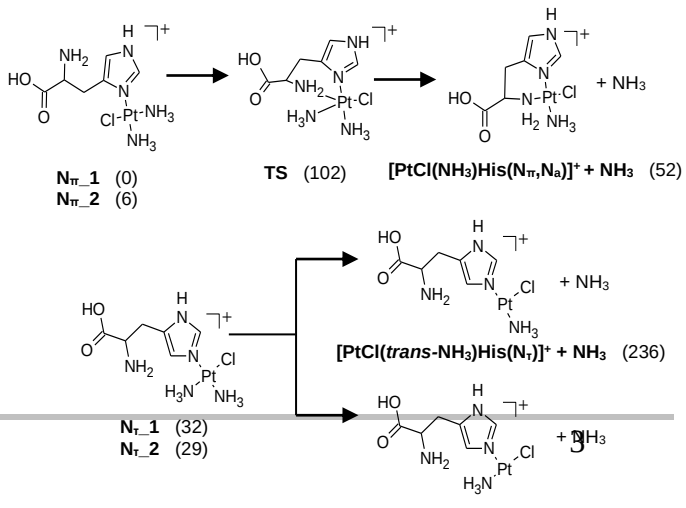

$\mathbf{N_\pi\_1}$ (0)
$\mathbf{N_\pi\_2}$ (6)
TS (102)
$[PtCl(NH_3)His(N_\pi,N_a)]^+ + NH_3$ (52)
$\mathbf{N_\tau\_1}$ (32)
$\mathbf{N_\tau\_2}$ (29)
$[PtCl(\mathit{trans}\text{-}NH_3)His(N_\tau)]^+ + NH_3$ (236)
$[PtCl(\mathit{cis}\text{-}NH_3)His(N_\tau)]^+ + NH_3$ (257)

Scheme 1. Fragmentation paths for $\mathbf{N_{\pi}}$ and $\mathbf{N_{\tau}}$ isomers. Relative enthalpies at 298 K in kJ mol^{-1} calculated at ωB97X-D/6-311+G** level are in parentheses.

In the X-H stretching frequency range of the IRMPD spectrum a prominent band at 3497 cm^{-1} arises from the NH stretching mode of the imidazole group and is a distinct feature in the IR spectra of $\mathbf{N_{\pi}}$ isomers. The geometry of $\mathbf{N_{\tau}}$ isomers allows the imidazole NH to be involved in a hydrogen bond, displacing the NH stretching to lower frequency. A second IRMPD band at 3565 cm^{-1} arises from the OH stretching mode of a 'free' hydroxyl group as in $\mathbf{N_{\pi}\_2}$, $\mathbf{N_{\tau}\_1}$ and $\mathbf{N_{\tau}\_2}$ isomers. Because these frequencies are isomer/conformer specific, one can exploit IRMPD kinetics to probe the relative population of isomeric species and any possible mutual conversion process.[30-34] The ion cloud overlap with the OPO/OPA laser beam has been verified using protonated His ($HisH^+$) as model ion and testing the IRMPD kinetics. The gas-phase structure of protonated histidine has been examined by IRMPD spectroscopy in the fingerprint range.[35] Protonation occurs on the imidazole group and low-lying conformers are characterized by at least one H-bond involving N_{π}-H.[35,36] In contrast, the N_{τ}-H bond is remote from the His chain and the calculated IR spectrum of the most stable conformer shows its frequency at 3466 cm^{-1} in fair agreement with the prominent IRMPD band at 3478 cm^{-1} (Figure S7). IRMPD kinetics performed at this frequency were based on recording the parent ion depletion ($HisH^+$ at *m/z* 156). The kinetics conform to a neat exponential decay (Figure S8) with k = 0.13 s^{-1} to ca. 97% depletion of the parent ion abundance. The nearly complete depletion suggests that in our experimental setup there is good overlap of the IR beam with the ion cloud at the examined frequency. In the specific case of $HisH^+$ ions the monoexponential decay indicates that either a single conformer is prevailing in the sampled mixture, or that distinct conformers display closely similar IRMPD activity or fast interconversion between different conformers is occurring. In the previously cited IRMPD study of $HisH^+$ ions in the fingerprint region it was shown that two distinct conformers are present, differing for the hydrogen bonding network at N_{π}-H, while both possessing a free N_{τ}-H.[35]

In order to gain an insight into the isomeric population of *cis*-$[PtCl(NH_3)_2(His)]^+$ ions, IRMPD kinetics have been monitored at the two distinct frequencies of 3497 and 3565 cm^{-1} and plotted in Figure 3.

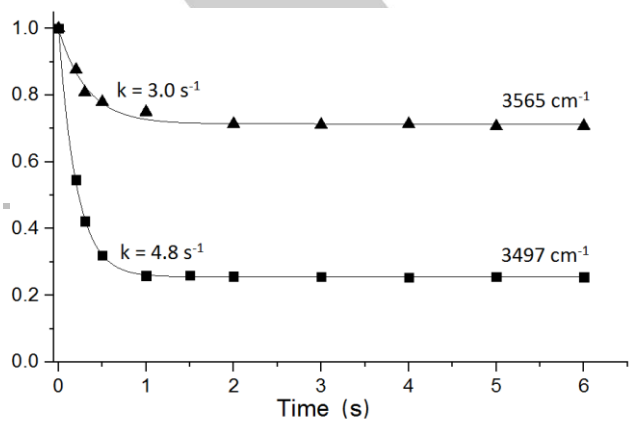

Figure 3. Decay of the parent ion *cis*-$[PtCl(NH_3)_2His]^+$ abundance plotted as a function of irradiation time. For each selected wavenumber the value of the kinetic constant is reported.

Both kinetics conform to a monoexponential decay with rate constants differing by less than a factor of 2 indicating that the photofragmentation process may involve the same or closely similar species. This behavior may be accounted for by a population of $\mathbf{N_{\pi}}$ conformers (such as $\mathbf{N_{\pi}\_1}$, $\mathbf{N_{\pi}\_2}$), characterized by comparable oscillator strength in the 3497 and 3565 cm^{-1} resonances and similar fragmentation thresholds. The photofragmentation kinetics do not account for the overall ion population, though, ending with an unreactive fraction of 25% and 70% at 3497 and 3565 cm^{-1}, respectively. In the IR spectra of $\mathbf{N_{\pi}\_1}$ and $\mathbf{N_{\pi}\_2}$ shown in Figure 1, one notes that $\mathbf{N_{\pi}\_1}$ is not IR active at 3565 cm^{-1}, in agreement with the reduced amplitude of the exponential decay at this frequency. The unreactive fraction at 3497 cm^{-1} may be related to the presence of the $\mathbf{N_{\tau}}$ conformers that present a red-shifted imidazole NH stretching due to the presence of strong H-bonds with either CO or NH_2 groups. Furthermore, IRMPD kinetics were performed at 3350 and 3392 cm^{-1}, probing modes that are not isomer specific (see Figure 1). In proximity with these frequencies, the ion cloud overlap has been verified on the IRMPD band at 3350 cm^{-1} of protonated dopamine (Figure S8). The results (Figure S9) confirm the presence of an unreactive fraction of ca. 25% of the parent ion suggesting the absence of IRMPD activity for the $\mathbf{N_{\tau}}$ conformers in the whole XH (X = C, N, O) stretching region. Thus, the obtained evidence leads us to assign a contribution of 25% for $\mathbf{N_{\tau}}$ isomers in the sampled *cis*-$[PtCl(NH_3)_2His]^+$ complexes. Hence, the analysis of the spectroscopic data in 3000-3700 cm^{-1} range supports the following outline: (i) $\mathbf{N_{\tau}}$ isomers do not appear to contribute to IRMPD activity, likely due to a high fragmentation threshold and limited photon density in the range accessed by the OPO/OPA laser; (ii) $\mathbf{N_{\pi}}$ conformers ($\mathbf{N_{\pi}\_1}$, $\mathbf{N_{\pi}\_2}$) account for the IRMPD signatures as shown by the IR spectra reported in Figure 1 and the mode assignment in Table S2; (iii) photodissociation kinetics provide a probe of isomer/conformer population showing that inactive N_{τ} isomers co-exist with N_{π} conformers characterized by a 'free' NH stretching at 3497 cm^{-1} of the imidazole group but differing for the presence of a 'free' OH stretching at 3565 cm^{-1} of the carboxylic functionality. Because only $\mathbf{N_{\pi}\_2}$ possesses the 'free' OH stretching and is IR active at 3565 cm^{-1}, the percentage of photofragmenting ions at this frequency may be assigned to the contribution of $\mathbf{N_{\pi}}$_2 in the ion population, amounting to ca. 30 %. Because both $\mathbf{N_{\pi}\_1}$ and $\mathbf{N_{\pi}\_2}$ contribute to the 75 % depletion at 3497 cm^{-1}, the fraction of $\mathbf{N_{\pi}\_1}$ may then be estimated to be ca. 45 %.

A note may be added about the broad band at 3125 cm^{-1}. The large width is consistent with the assignment to OH and asymmetric NH_3 stretching modes involved in hydrogen bonding (Table S2). However, in this case the anharmonic frequency calculations appear to overestimate the expected red shift. Theoretically overestimated red shifts of hydrogen-bonded OH and NH stretches are however documented.[37-38]

A comprehensive view of higher energy conformers, including species that are not expected to contribute significantly to the sampled population, for the two families of N_π and N_τ isomers is provided in Figure S5, while Figure S10 shows their IR harmonic spectra together with the experimental IRMPD spectrum. Table S1 summarizes the thermodynamic data for all tested species.

It is also conceivable that the histidine ligand in *cis*-$[PtCl(NH_3)_2(His)]^+$ ions may bind the metal by donor atoms other than N_π and N_τ belonging to the imidazole group. In this view a computational survey has examined a variety of plausible candidates whose structures are reported in Figure S6. Attack by the amino nitrogen yields species named $\mathbf{N_aH_a}$ and $\mathbf{N_aH_i}$ differing for the position of a proton which moves from the amino nitrogen in $\mathbf{N_aH_a}$ to the imidazole aza group in $\mathbf{N_aH_i}$. A neutral carboxylic group is coordinated to Pt^{II} in the species labeled **OH** while the proton formerly on oxygen is shifted to the amino or imidazole nitrogen to yield $\mathbf{OH_a}$ and $\mathbf{OH_i}$. Thermodynamic data for the named species are collected in Table S1 and the calculated IR spectra are reported in Figure S10. None of these spectra compares well with the experimental IRMPD spectrum. In particular, it is worth noting that these isomers are characterized by C=O stretching frequencies appreciably lower than the experimental band at 1755 cm^{-1}. Thus, the finding that the ion population sampled at this resonance undergoes thorough photofragmentation speaks against a significant contribution of any of these alternative isomers. For the same reason, it is highly unlikely that any of them may be identified as the non-fragmenting species in the OPO/OPA region.

Conclusions

In conclusion, ESI has allowed us to reveal the primary complex involving cisplatin coordination to histidine, delivering it to the gas-phase for analysis by mass spectrometry and IR spectroscopy. The *cis*-$[PtCl(NH_3)_2(His)]^+$ complex has shown metal coordination engaging the N_π and N_τ imino nitrogens of the imidazole group. The so-formed $\mathbf{N_\pi}$ and $\mathbf{N_\tau}$ isomers result from cisplatin attack to either one of the same aza functional group of the imidazole ring, differing for the position relative to the amino acid side chain, existing in the two tautomers of histidine. Both sites are expected to bind the metal, as reported for similar platinum(II) complexes.[10] Moreover, we were able to give an estimate of the individual contributions of $\mathbf{N_\pi}$ and $\mathbf{N_\tau}$ isomers and conformers relying on IRMPD kinetic measurements. Ultimately, one may assign approximate fractions for the species partaking in the sampled population, namely 45% for $\mathbf{N_\pi\_1}$, 30% for $\mathbf{N_\pi\_2}$, and 12.5% for both $\mathbf{N_\tau\_1}$ and $\mathbf{N_\tau\_2}$. The latter assignment is obtained from the 25% fraction that is not IRMPD active in the XH stretching range and assigned to $\mathbf{N_\tau\_1}$ and $\mathbf{N_\tau\_2}$ isomers, on account of their nearly equal free energy at room temperature (see Table 1). Thus, a linear combination of calculated IR spectra can be derived, considering the contribution of all species in the fingerprint region while only $\mathbf{N_\pi\_1}$ and $\mathbf{N_\pi\_2}$ contribute to the observed IR spectrum in the XH stretching range. This experimentally weighted average of the IR spectra of the sampled N_π and N_τ isomeric population is depicted in the upper panel of Figure 4, showing good agreement with the experimental IRMPD spectrum (lower panel), especially if one considers that IRMPD intensities reflect the efficiency of the photofragmentation process and are not a direct reflection of a linear IR spectrum, though frequently showing close correspondence.[11-13] Indeed, an accurate reproduction of IR intensities still represents a challenge for computations. It is also worth noting that no corrections or scaling factors have been used in the calculated anharmonic spectra. Notably, the relative fraction of $\mathbf{N_\pi}$ and $\mathbf{N_\tau}$ isomers sampled in the gas-phase does not respond to the respective gas-phase stabilities. It rather reveals the outcome of the cisplatin reaction in solution, reflecting the kinetically trapped $\mathbf{N_\pi}$ and $\mathbf{N_\tau}$ ratio. Indeed, several authors have reported that in a variety of instances the ion population sampled by ESI reflects kinetic trapping rather than being governed by the gas phase thermodynamics.[39-41] The increased relative stability of $\mathbf{N_\tau}$ relative to $\mathbf{N_\pi}$ isomers when solvation is accounted for lends further support to this line of reasoning,[42] although thermodynamic considerations alone do not provide a uniform rationale to the reactivity patterns observed in the solution chemistry of platinum(II) complexes.[10]

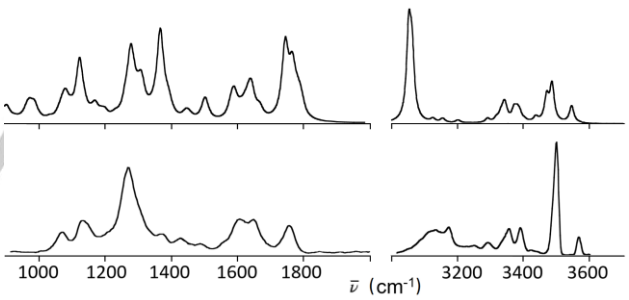

Figure 4. IRMPD spectrum of *cis*-$[PtCl(NH_3)_2His]^+$ (bottom panel) compared to the averaged linear anharmonic IR spectra (upper panel). The contribution of all species, $\mathbf{N_t\_1/N_t\_2}$ and $\mathbf{N_\pi\_1/N_\pi\_2}$, is involved in the fingerprint region while only $\mathbf{N_\pi\_1}$ and $\mathbf{N_\pi\_2}$ contribute to the observed IR spectrum in the XH stretching range. No correction or scaling factors were used in the computed spectra.

This study shedding light on the early step of the cisplatin reaction with histidine and histidine-containing peptides and proteins, paves the way towards a thorough appraisal of the cisplatin interaction with amino acid targets at the molecular level.

Experimental Section

- Mass spectrometric experiments

Cisplatin and L-histidine (His) used in this work were research grade products obtained from a commercial source (Sigma-Aldrich s.r.l Milan, Italy), used without further purification. Cisplatin and His were solubilized to prepare separate aqueous solutions in the millimolar range. These mother solutions were mixed in 1:1 molar ratio and diluted in 1:1 methanol/water to reach the concentration of 5×10^{-5} M in each compound. The solution was submitted to electrospray ionization (ESI) by direct infusion using a syringe pump at a typical flow rate of 180 µL h^{-1}. Mass spectra and collision induced dissociation (CID) experiments have been recorded on a hybrid triple quadrupole linear ion trap mass spectrometer (2000 Q-TRAP Applied Biosystems). In this instrument the ESI conditions employed were: curtain gas at 20.0 psi, ion source gas at 20.0 psi, declustering potential at 80 V and entrance potential at 8 V. Nitrogen was used as collision gas at a nominal pressure of 2.7 10^{-5} mbar. Moderate changes (by a factor of five) in the pressure of the collision gas do not significantly affect the fragmentation behavior, suggesting prevailing single collision conditions. The isotopic cluster centered at *m/z* 418-422 is assigned to *cis*-$[PtCl(NH_3)_2(His)]^+$ ions, displaying the characteristic isotopic pattern. For the sake of simplicity, we refer to the platinum complexes by naming the *m/z* value of the species containing ^{194}Pt and ^{35}Cl isotopes, corresponding to the first major ion in the isotopic cluster. Thus, the *cis*-$[PtCl(NH_3)_2(His)]^+$ complex is associated to just *m/z* 418.
High resolution mass analysis of the isotopic pattern of Pt and Cl corresponding to *cis*-$[PtCl(NH_3)_2(His)]^+$ ions was acquired using a 7T SolariX hybrid Fourier transform - ion cyclotron resonance (FT-ICR) mass spectrometer (Bruker Daltonics, Bremen, Germany) sited at the Laboratoire de Chimie Moléculaire, École Polytechnique, Palaiseau, France. Elemental compositions for all peaks were obtained using the instrument software DataAnalysis and characterized by a tolerance below 5 ppm.

- Infra Red Multiple Photon Dissociation (IRMPD) spectroscopy

IRMPD spectroscopy was run in two frequency ranges, namely 900-1900 cm^{-1} and 3000-3700 cm^{-1}, using two experimental setups, both based on the coupling of ion trap mass spectrometry with the beamline of a tunable IR laser. The lower wavenumber "fingerprint" range, 900-1900 cm^{-1}, was investigated at the Centre Laser Infrarouge d'Orsay (CLIO). The FEL radiation enters the cell of a hybrid FT-ICR tandem mass spectrometer (APEX-Qe Bruker Daltonics),[43] equipped with a 7.0 T actively shielded magnet and a quadrupole−hexapole interface for mass-filtering and ion accumulation, under the control of the commercial software APEX 1.0. The ion studied in this work, *cis*-$[PtCl(NH_3)_2(His)]^+$, was mass selected in the quadrupole and accumulated for 1.0 s in the hexapole, containing Argon as buffer gas, in order to cool it prior to its transfer into the ICR cell. The isolated ions were then irradiated for 250-500 ms with the IR FEL light and the products of the excitation were mass analyzed. The FEL electron energy was set at 43.5 and 44.4 MeV to optimize the laser power in the IR range of interest. The FEL radiation is delivered in trains of 9 µs long macropulses at a repetition rate of 25 Hz. A macropulse comprises 600 micropulses, each few ps long. Under the operational conditions the average laser power was 1200 mW corresponding to a macropulse energy of 50 mJ.
IRMPD spectroscopy in the X-H (X = C, N, O) stretching range were recorded on an apparatus assembled at the Università di Roma "La Sapienza" where a modified commercial ion trap mass spectrometer (Bruker Esquire 6000) is coupled with an optical parametric oscillator/amplifier (OPO/OPA, LaserVision, Bellevue, WA, U.S.A).[44] This laser system is pumped by the 1064 nm fundamental of a Nd:YAG laser (Continuum Surelite II) operating at 10 Hz repetition rate and delivering 600 mJ per pulse (4–6 ns long). The typical output energy of the OPO/OPA was ca. 23 mJ/pulse in the spectral range of investigation with 3 - 4 cm^{-1} bandwidth.
In the ion trap, ions are accumulated for 20 ms, mass selected and submitted to irradiation from 0.3 to 10 s. The laser wavelength was continuously changed at a speed of 0.1 cm^{-1} s^{-1}.
In either range, the mass spectrum was typically obtained from an accumulation over 3-4 scans.
The IRMPD process consists in a first absorption of a photon resonant with the vibrational mode of a mass selected ion. Generally, the energy delivered to the ion is not enough to obtain fragmentation, therefore subsequent absorption steps need to occur while the absorbed energy is being distributed over all the vibrational modes through intramolecular vibrational redistribution (IVR), until the dissociation threshold is reached. The *cis*-$[PtCl(NH_3)_2(His)]^+$ (*m/z* 418) ion fragments by loss of ammonia yielding $[PtCl(NH_3)(His)]^+$ (*m/z* 401). The IR action spectra are obtained by plotting the photofragmentation yield $R = -\ln I_p/(I_p + \Sigma I_f)$, where I_p and ΣI_f are the parent and sum of the fragment ion intensities, respectively, as a function of the radiation wavenumber.[30] The yield is not normalized with laser power along the IRMPD spectrum, rather, the laser power is plotted on top of the experimental spectrum.
The IRMPD kinetics were obtained varying the irradiation time of the mass selected ion at a fixed IR frequency and plotting the percent of parent ion abundance as a function of time.

-Theoretical calculations

An exploration of the conformer distribution for plausible isomers of *cis*-$[PtCl(NH_3)_2(His)]^+$ was made using a Monte Carlo search following a path that biases in favor of low energy conformers and employing the semi-empirical method PM6.[45] The tool Conformer Distribution as implemented in the software suite Spartan'10 was used.[46] The low energy conformers have been re-optimized using the Gaussian 09 Rev D.01 package at the B3LYP/6-311
+G** level of theory.[47-49] In order to take into account relativistic effects, proven to be important to describe heavy atoms like platinum,[50] the LanL2TZ effective core potential (ECP)), that contains the LANL2 relativistic ECP of Hay and Wadt and a flexible triple-zeta basis set, was used for the platinum atom in all the calculations.[51] Subsequently, the whole set of geometries was submitted to computations of the harmonic vibrational frequency, in order to obtain linear IR spectra and thermodynamic data. The analysis of the vibrational frequencies is used to characterize the optimized structures 09 Rev D.01 package at the B3LYP/6-311+G** level of theory.[47-49] as local minima, if no imaginary frequencies are present, or as transition state (with one imaginary frequency corresponding to the motion along the reaction coordinate). Moreover, selected geometries were submitted to anharmonic vibrational analysis according to vibrational perturbation theory at the second order, VPT2, as implemented in Gaussian09,[52] to account for anharmonicity effects that may affect in particular vibrational modes characteristic of H-bonded molecular groups.
All the theoretical IR spectra presented in this paper are calculated at the B3LYP/6-311+G** level of theory. The hybrid DFT functionals are known to overestimate the computed frequencies. To overcome the problem the harmonic IR frequencies have been scaled by 0.974 and 0.957 in the fingerprint region and in the X-H (X= C, N, O) stretch region, respectively. These values are in line with those used in previous work employing the same level of theory.[14,15] Calculated anharmonic frequencies are presented unscaled. A Gaussian shape, having a fwhm of 20 cm^{-1} in the fingerprint range and of 5 cm^{-1} in the X-H stretching range, was adopted to simulate the experimental spectrum.
Low-lying conformers of the selected isomers have been re-optimized using the ωB97X-D and B3LYP-D3 functionals and the same basis set used above, in order to include the contribution of dispersion effects. In particular the ωB97X-D hybrid functional that includes the long range correction and the dispersion correction following Grimme's work with a modified damping function,[26] has proven to be a proper tool to calculate

the energies and geometries of platinum complexes.[27] In order to obtain thermal corrections, harmonic vibrational frequencies of the newly optimized geometries have been calculated at the same level.
Single point energy calculations were also performed on selected geometries at the MP2/cc-pVTZ level of theory using cc-pVTZ-PP as pseudopotential for the platinum atom in order to evaluate the importance of correlation with post-Hartree-Fock methods. MP2 thermodynamic parameters were obtained by using B3LYP-derived thermal corrections, thus yielding MP2/cc-pVTZ(-PP)//B3LYP/6-311+G** data.
Solvation effects were calculated at the B3LYP and ωB97X-D level of theory for selected species using the Polarizable Continuum Model (PCM) as implemented in Gaussian09 employing water as model solvent.

Acknowledgements

This work was supported by the Università degli Studi di Roma "La Sapienza" and by the European Commission (CLIO project IC14-011). We are grateful to Philippe Maitre, Jean-Michel Ortega, Debora Scuderi, Vincent Steinmetz and the CLIO team and to Annito Di Marzio for experiments at the OPO/OPA laser. MEC thanks Gilles Frison for high resolution mass measurements at the SolariX FT-ICR instrument, Ecole Polytechnique, Palaiseau, France.

Keywords: cisplatin • antitumor agents • electrospray ionization mass spectrometry • structure elucidation • isomerism

[1] T. C. Johnstone, K. Suntharalingam, S. J. Lippard, *Chem. Rev.* **2016**, *116*, 3436-3486.
[2] Harper, A. M. Krause-Heuer, M. P. Grant, M. Manohar, K. B. Garbutcheon-Singh, J. R. Aldrich-Wright, *Chem.-Eur. J.* **2010**, *16*, 7064-7077.
[3] P. J. Dyson, G. Sava, *Dalton Trans.* **2006**, 1929-1933.
[4] D. Wang, S. J. Lippard, *Nat. Rev. Drug Discovery* **2005**, *4*, 307-320.
[5] A. V. Klein, T. W. Hambley, *Chem. Rev.* **2009**, *109*, 4911-4920.
[6] R. Wirth, J. D. White, A. D. Moghaddam, A. L. Ginzburg, L. N. Zakharov, M. M. Haley, V. J. DeRose, *J. Am. Chem. Soc.* **2015**, *137*, 15169-15175.
[7] G. Sava, G. Jaouen, E. A. Hillard, A. Bergamo, *Dalton Trans.* **2012**, *41*, 8226-8234.
[8] A. Casini, J. Reedijk, *Chem. Sci.* **2012**, *3*, 3135-3144.
[9] V. Saudek, H. Pivcova, D. Noskova, J. Drobnik, *J. Inorg. Biochem.* **1985**, *23*, 55-72.
[10] T. G. Appleton, *Coord. Chem. Rev.* **1997**, *166*, 313-359.
[11] M. A. Duncan, *J. Phys. Chem. A* **2012**, *116*, 11477-11491.
[12] J. Roithova, *Chem. Soc. Rev.* **2012**, *41*, 547-559.
[13] J. R. Eyler, *Mass Spectrom. Rev.* **2009**, *28*, 448-467.
[14] B. Chiavarino, M. E. Crestoni, S. Fornarini, D. Scuderi, J. Y. Salpin, *J. Am. Chem. Soc.* **2013**, *135*, 1445-1455.
[15] B. Chiavarino, M. E. Crestoni, S. Fornarini, D. Scuderi, J. Y. Salpin, *Inorg. Chem.* **2015**, *54*, 3513-3522.
[16] A. De Petris, A. Ciavardini, C. Coletti, N. Re, B. Chiavarino, M. E. Crestoni, S. Fornarini, *J. Phys. Chem. Lett.* **2013**, *4*, 3631-3635.
[17] D. Corinti, C. Coletti, N. Re, B. Chiavarino, M. E. Crestoni, S. Fornarini, *Chem.-Eur. J.* **2016**, *22*, 3794-3803.
[18] C. C. He, B. Kimutai, X. Bao, L. Hamlow, Y. Zhu, S. F. Strobehn, J. Gao, G. Berden, J. Oomens, C. S. Chow, M. T. Rodgers, *J. Phys. Chem. A* **2015**, *119*, 10980-10987.
[19] B. E. Ziegler, R. A. Marta, M. B. Burt, T. B. McMahon, *Inorg. Chem.* **2014**, *53*, 2349-2351.
[20] M. Citir, C. S. Hinton, J. Oomens, J. D. Steill, P. B. Armentrout, *J. Phys. Chem. A* **2012**, *116*, 1532-1541.
[21] T. E. Hofstetter, C. Howder, G. Berden, J. Oomens, P. B. Armentrout, *J. Phys. Chem. B* **2011**, *115*, 12648-12661.
[22] H. Lavanant, E. Hecquet, Y. Hoppilliard, *Int. J. Mass Spectrom.* **1999**, *185*, 11-23.
[23] R. K. Sinha, D. Scuderi, P. Maitre, B. Chiavarino, M. E. Crestoni, S. Fornarini, *J. Phys. Chem. Lett.* **2015**, *6*, 1605-1610.
[24] A. Filippi, C. Fraschetti, S. Piccirillo, F. Rondino, B. Botta, I. D'Acquarica, A. Calcaterra, M. Speranza, *Chem. Eur. J.* **2012**, *18*, 8320-8328.
[25] IUPAC, *Compendium of Chemical Terminology, 2nd ed. (the "Gold Book")* (Eds.: A. D. McNaught, A. Wilkinson), Blackwell Scientific Publications, Oxford, **1997**.
[26] J. D. Chai, M. Head-Gordon, *Phys. Chem. Chem. Phys.* **2008**, *10*, 6615-6620.
[27] Y. Minenkov, A. Singstad, G. Occhipinti, V. R. Jensen, *Dalton Trans.* **2012**, *41*, 5526-5541.
[28] J. Oomens, J. D. Steill, B. Redlich, *J. Am. Chem. Soc.* **2009**, *131*, 4310-4319.
[29] R. Paciotti, C. Coletti, N. Re, D. Scuderi, B. Chiavarino, S. Fornarini, M. E. Crestoni, *Phys. Chem. Chem. Phys.* **2015**, *17*, 25891-25904.
[30] J. S. Prell, J. T. O'Brien, E. R. Williams, *J. Am. Soc. Mass Spectrom.* **2010**, *21*, 800-809.
[31] J. S. Prell, T. M. Chang, J. A. Biles, G. Berden, J. Oomens, E. R. Williams, *J. Phys. Chem. A* **2011**, *115*, 2745-2751.
[32] J. S. Prell, T. M. Chang, J. T. O'Brien, E. R. Williams, *J. Am. Chem. Soc.* **2010**, *132*, 7811-7819.
[33] O. Hernandez, B. Paizs, P. Maitre, *Int. J. Mass Spectrom.* **2015**, *377*, 172-178.
[34] J. Schmidt, S. R. Kass, *J. Phys. Chem. A* **2013**, *117*, 4863-4869.
[35] M. Citir, C. S. Hinton, J. Oomens, J. D. Steill, P. B. Armentrout, *Int. J. Mass Spectrom.* **2012**, *330*, 6-15.
[36] V. Riffet, G. Bouchoux, *Phys. Chem. Chem. Phys.* **2013**, *15*, 6097-6106.
[37] M. Broquier, F. Lahmani, A. Zehnacker-Rentien, V. Brenner, P. Millier, A. Peremans, *J. Phys. Chem. A* **2001**, *105*, 6841-6850.
[38] K. Mackeprang, H. G. Kjaergaard, T. Salmi, V. Hänninen, L. Halonen, *J. Chem. Phys.* **2014**, *140*, 184309-1/9.
[39] A. Zehnacker, *Int. Rev. Phys. Chem*. **2014**, *33*, 151-207.
[40] L. Voronina, T. R. Rizzo, *Phys. Chem. Chem. Phys.* **2015**, *17*, 25828-25836.
[41] W. S. Hopkins, R. A. Marta, V. Steinmetz, T. B. McMahon, *Phys. Chem. Chem. Phys.* **2015**, *17*, 28548-28555.
[42] We are grateful to a reviewer for highlighting this point.
[43] J. M. Bakker, T. Besson, J. Lemaire, D. Scuderi, P. Maitre, *J. Phys. Chem. A* **2007**, *111*, 13415-13424.
[44] R. K. Sinha, P. Maitre, S. Piccirillo, B. Chiavarino, M. E. Crestoni, S. Fornarini, *Phys. Chem. Chem. Phys.* **2010**, *12*, 9794-9800.
[45] J. J. P. Stewart, *J. Mol. Model.* **2007**, *13*, 1173-1213.
[46] *Spartan 10*, Program for Calculation of Molecular Properties; Wavefunction Inc.: Irvine, CA, USA.
[47] M. J. Frisch, G. W. Trucks, H. B. Schlegel, G. E. Scuseria, M. A. Robb, J. R. Cheeseman, G. Scalmani, V. Barone, B. Mennucci, G. A. Petersson, H. Nakatsuji, M. Caricato, X. Li, H. P. Hratchian, A. F. Izmaylov, J. Bloino, G. Zheng, J. L. Sonnenberg, M. Hada, M. Ehara, K. Toyota, R. Fukuda, J. Hasegawa, M. Ishida, T. Nakajima, Y. Honda, O. Kitao, H. Nakai, T. Vreven, J. A. Montgomery Jr., J. E. Peralta, F. Ogliaro, M. J. Bearpark, J. Heyd, E. N. Brothers, K. N. Kudin, V. N. Staroverov, R. Kobayashi, J. Normand, K. Raghavachari, A. P. Rendell, J. C. Burant, S. S. Iyengar, J. Tomasi, M. Cossi, N. Rega, N. J. Millam, M. Klene, J. E. Knox, J. B. Cross, V. Bakken, C. Adamo, J. Jaramillo, R. Gomperts, R. E. Stratmann, O. Yazyev, A. J. Austin, R. Cammi, C. Pomelli, J. W. Ochterski, R. L. Martin, K. Morokuma, V. G. Zakrzewski, G. A. Voth, P. Salvador, J. J. Dannenberg, S. Dapprich, A. D. Daniels, Ö. Farkas, J. B. Foresman, J. V. Ortiz, J. Cioslowski, D. J. Fox, Gaussian, Inc., Wallingford, CT, USA, **2009**.
[48] C. T. Lee, W. T. Yang, R. G. Parr, *Phys. Rev. B* **1988**, *37*, 785-789;
[49] A. D. Becke, *J. Chem. Phys.* **1993**, *98*, 5648-5652.
[50] H. Schwarz, *Angew. Chem. Int. Edit.* **2003**, *42*, 4442-4454.
[51] P. J. Hay, W. R. Wadt, *J. Chem. Phys.* **1985**, *82*, 299-310.
[52] V. Barone, *J. Chem. Phys.* **2005**, *122,* 014108.

Entry for the Table of Contents (Please choose one layout)

Layout 1:

ARTICLE

Cisplatin attack to L-histidine, a prime biological target, is directed to N_{π} and N_{τ} atoms of the imidazole group in proportions revealed by IRMPD kinetics.

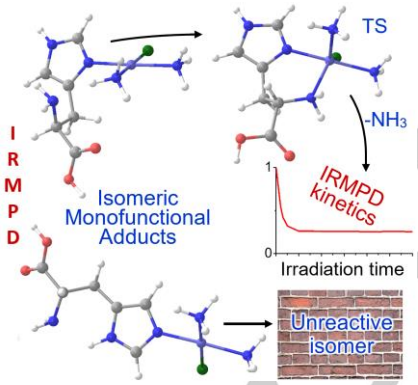

*Author(s), Corresponding Author(s)**

Page No. – Page No.

Title